

The Emergence of Lines of Hierarchy in Collective Motion of Biological Systems

James M. Greene¹, Eitan Tadmor², Ming Zhong³

¹ Department of Mathematics, Clarkson University, Potsdam, NY, United States

² Department of Mathematics and Institute for Physical Science & Technology, University of Maryland, College Park, MD, United States

³ Department of Applied Mathematics, Illinois Institute of Technology, Chicago, IL, United States

E-mail: tadmor@umd.edu

Abstract. The emergence of large scale structures in biological systems, and in particular the formation of lines of hierarchy, is observed in many scales, from collections of cells to groups of insects to herds of animals. Motivated by phenomena in chemotaxis and phototaxis, we present a new class of alignment models which exhibit alignment into lines. The spontaneous formation of such “fingers” can be interpreted as the emergence of leaders and followers in a system of identically interacting agents. Various numerical examples are provided, which demonstrate emergent behaviors similar to the “fingering” phenomenon observed in some phototaxis and chemotaxis experiments; this phenomenon is generally known as a challenging pattern to capture for existing models. The novel pairwise interactions provides a fundamental mechanism by which agents may form social hierarchy across a wide range of biological systems.

Key Words: Collective Dynamics, Emergent Behavior, Lines of Hierarchy, Active Particles

Acknowledgments

Research of ET was supported in part by ONR grant N00014-2112773. Research of MZ was supported in part by NSF grant CCF-AF-2225507.

Submitted to: *Phys. Biol.*

1. Introduction — emergent phenomena in biological systems

Emergent phenomena in collective dynamics are observed in a wide range of biological systems and across different scales — from cells to bacteria, from insects to fish, from humans to mammals. Accordingly, it has been a topic of scientific interest in a wide range of disciplines, including biology, ecology, physics, mathematics, and computer science [1]. In this context, one is concerned with “active particles” which consists of living agents (and likewise, certain types of mechanical agents), equipped with senses and sensors, with which they probe the environment. These are responsible for small scale pairwise interactions. The phenomenon of emergence is observed when a crowd of agents, driven by those small scale interactions, is self-organized into large scale formations: ants form colonies, insects swarm, birds fly in flocks, mobile networks coordinate a rendezvous or create traffic jams, human opinions evolve into parties and so on. Thus, with no apparent central control or a built-in bias in the dynamics, the question arises — where does this unity from within come from? what is behind the seemingly spontaneous self-organization?

Let $\phi(\mathbf{x}_i, \mathbf{x}_j)$ denote the amplitude of pairwise interaction of agents positioned at \mathbf{x}_i and \mathbf{x}_j . Recent studies of collective dynamics identified different classes of interaction kernels which play a decisive role in governing the different features of their emergent behavior, [2, 3, 4]. These include metric kernels depending on the metric distance between agents, [5, 6],

$$\phi(\mathbf{x}_i, \mathbf{x}_j) = \phi(|\mathbf{x}_i - \mathbf{x}_j|). \quad (1)$$

Then there are topologically-based kernels depending on how crowded is the region enclosed between agents positioned at \mathbf{x}_i and \mathbf{x}_j , rather

than their metric distance, [7, 8],

$$\phi(\mathbf{x}_i, \mathbf{x}_j) = \phi\{\#k : \mathbf{x}_k \in \mathcal{C}(\mathbf{x}_i, \mathbf{x}_j)\}. \quad (2)$$

Further, we distinguish between the class of long-range heavy-tailed kernels, $\int_0^\infty k(r)dr = \infty$, expressed in terms of their radial envelope, [9, 10]

$$k(r) := \min\{\phi(\mathbf{x}, \mathbf{x}') : |\mathbf{x} - \mathbf{x}'| \leq r\}, \quad (3)$$

and singular-headed kernels, $k(r) = r^{-\beta}$, $\beta > 0$, [11, 12, 13] vs. short range, compactly supported kernels, [14], $k(r) \lesssim \mathbf{1}_{r \leq r_0}$.

Our primary interest is in self-organization which is independent of external forces/stimuli; for a mathematical analysis of the latter see e.g. [15].

1.1. Attraction, repulsion, alignment

One classifies three main types of pairwise interactions which govern the emergent phenomena observed in biological systems, namely — attraction, repulsion and alignment, [16, 17, 18]. The first two main features are attraction which acts as a cohesion towards average position of neighboring agents, while repulsion steers to avoid collisions. These are familiar from particle dynamics. A typical first order attraction-repulsion dynamics reads

$$\dot{\mathbf{x}}_i(t) = -\frac{1}{|\mathcal{N}_i(t)|} \sum_{j \in \mathcal{N}_i(t)} \phi(\mathbf{x}_i, \mathbf{x}_j)(\mathbf{x}_i - \mathbf{x}_j). \quad (4)$$

Here, the agent positioned at \mathbf{x}_i interacts with its neighbors at $\mathcal{N}_i(t) := \{j : \phi(\mathbf{x}_i(t), \mathbf{x}_j(t)) \neq 0\}$, of size $|\mathcal{N}_i|$. Thus, with the pre-factor normalization in (4), it can be interpreted as a local environmental averaging of positions. Short-range vs. long-range kernels translate into local vs. global neighborhoods. Attraction and repulsion are dictated by the positive, and respectively negative, parts of $\phi_{ij} = \phi(\mathbf{x}_i, \mathbf{x}_j)$. The balance between attraction and repulsion is responsible for the phenomenon of

aggregation, where crowd of agents is self-organized into one or more large scale stationary clusters with observable geometric configuration. Different kernels $\phi(\cdot, \cdot)$ lead to a great variety of different limiting configurations. These are observed in cell biology, with tissue formation (mediated by cell-to-cell recognition and cell adhesion) being the prototypical example [19]; cell aggregation also plays a fundamental role in cellular differentiation [20], proliferation [21, 22], and viability [22, 23]. We mention on passing the important role aggregation plays in cellular viability, e.g., when it is utilized in biofilms as a survival mechanism for bacterial cells, and for cellular adhesion in chemo- and radio-resistance [24, 25, 26, 27]. Aggregates of cells also commonly coordinate their movement to collectively migrate; prominent biological processes displaying this behavior are wound healing and cancer invasion [28], as well as chemotaxis and phototaxis [29, 30]. Aggregation is of course not limited to cells; thus for example, many species of insects (e.g. monarch butterflies overwintering) and animals forming complex social structures for a diverse set of evolutionary reasons [31].

A third main feature in emergent dynamics is driven alignment — the steering towards average heading of neighboring agents. A typical second-order alignment dynamics reads

$$\dot{\mathbf{p}}_i(t) = -\frac{\tau}{|\mathcal{N}_i(t)|} \sum_{j \in \mathcal{N}_i(t)} \phi(\mathbf{x}_i, \mathbf{x}_j)(\mathbf{p}_i - \mathbf{p}_j). \quad (5)$$

Here, $\tau > 0$ is a fixed scaling parameter, and \mathbf{p}_i stands for the velocity of the agent positioned at $\mathbf{x}_i(t)$, [5, 6], $\mathbf{p}_i(t) \mapsto \mathbf{v}_i(t) := \dot{\mathbf{x}}_i(t)$, or its orientation, [14, 32, 33], $\mathbf{p}_i(t) \mapsto \omega_i(t) := \mathbf{v}_i(t)/|\mathbf{v}_i(t)| \in \mathbb{S}^{d-1}$. In a typical case of long-range interactions in a crowd of N agents, $|\mathcal{N}_i| = N$; one can adjust to short- and long-range interactions, replacing $|\mathcal{N}_i| \mapsto \sum_j |\phi(\mathbf{x}_i, \mathbf{x}_j)|$, [34]. The alignment encoded in (5) describes en-

vironmental averaging of velocities/orientations. Alignment may be either local or global, depending on the heavy-tailed scale of the interaction kernel. Alignment governs emergent phenomena of flocking or swarming, found in animal populations [35], in which agents attempt to align their heading and/or speed in a large scale coordinated movement. Schools of fish [36, 37, 38], flocks of birds [39, 40, 41, 42], and herds of animals [43] are some of the most well-known examples. We mention on passing the evolutionary roles played by flocking are diverse and species dependent: examples include reproductive efficiency, predation avoidance, and route learning in migration, [44, 45, 46]. Flocking can manifest itself via synchronization, in which pairwise interactions of agents are coordinated in time into large scale crowd oscillations. Well-known examples include the frequency of flashing of firefly lights [47], the “chorusing” behavior of some species of crickets [48], and the firing of neuron cells [49]. Flocking occurs in behavioral contexts as well, with consensus building being an emergent phenomenon in opinion dynamics [50]. It is realized on many different scales, from populations of cells to populations of humans [51].

The full complexity of self organization observed in biological systems is realized when combining attraction, repulsion and alignment. This was originally advocated in the pioneering work of Reynolds [16] for realistic simulation of boids – birds like objects. Reynolds’ model remains one of the most commonly utilized methods of describing collective motion, with extensions proposed to incorporate the effect of pheromone signaling [52] and obstacle avoidance [53], as well as a motivation for development of particle swarm optimization [54]. The incorporation of social hierarchy via leadership has also been explicitly incorporated into Reynolds’ rules for boids using an additional steering force which allows agents to change the course of the

flock based on the agent's position with respect to the flock [55]. We note that although most boids models are presented as discrete velocity updates rules, they typically can be translated to either deterministic or discrete second-order systems (see Section 3.2).

A systematic framework for combining attraction, repulsion and alignment mechanisms, is offered by anticipation dynamics induced by a radial potential U , and acting at the 'anticipated positions', $\mathbf{x}_i^\tau := \mathbf{x}_i + \tau \mathbf{v}_i$, [56] (here we make the simplification of long-range interactions $|\mathcal{N}_i| = N$),

$$\dot{\mathbf{v}}_i(t) = -\frac{1}{N} \sum_{j=1}^N \nabla_i U(|\mathbf{x}_i^\tau - \mathbf{x}_j^\tau|). \quad (6)$$

Expanding at the small "anticipated time" $t + \tau$, $\tau \ll 1$, one finds

$$\begin{aligned} \dot{\mathbf{v}}_i(t) = & -\frac{1}{N} \sum_j \phi_{ij}(\mathbf{x}_i - \mathbf{x}_j) \\ & + \frac{\tau}{N} \sum_j \Phi_{ij}(\mathbf{v}_j - \mathbf{v}_i). \end{aligned} \quad (7)$$

Here, attraction and repulsion are dictated by $\phi_{ij} := U'(|\mathbf{x}_i - \mathbf{x}_j|)/|\mathbf{x}_i - \mathbf{x}_j|$, and alignment is dictated by the Hessian, $\Phi_{ij} = D^2 U(|\mathbf{x}_i - \mathbf{x}_j|)$, with a scalar leading order term $\psi_{ij} = U''(|\mathbf{x}_i - \mathbf{x}_j|)$. Thus, for example, a standard U-shape potential-based anticipation dictates a 3Zone dynamics in three concentric regions, ranging from interior repulsion, $U' < 0$, through intermediate alignment where $U' \sim 0$ and surrounding with exterior attraction $U' > 0$. Such 3Zone dynamics is encountered in many models for flocking and swarming. For example, many species of insects exhibit swarming behavior in which their motion is self-organized into approximately concentric trajectories, known as milling, or vortex formation, [57]. This enables the insects to carry out specific tasks in the form of collective intelligence. Examples of swarming include the marching of locust nymphs [58, 59]

and lane formation and obstacle avoidance of army ants [33]. Milling is most commonly associated with fish populations during schooling and mating rituals [60, 32]. It also occurs in cell clusters [61, 62], and also less frequently in ants during extreme conditions [63].

Finally we note that although not a focus of the present work, understanding collective motion for biological crowds has numerous applications in the engineering sciences. Examples include mobile sensing networks and the utilization of cooperative unmanned aerial vehicles (UAVs) [64, 65, 66, 67, 68]. who have only recently begun to develop quantitative theories of collective motion [69].

1.2. A new collective model for fingering

Certain forms of emergent behavior can be classified as possessing degrees of social hierarchy, where individual agents conform to distinct roles. As with all emergent behavior, hierarchy can arise across a vast range of scales, from small groups of cells (e.g. in cell migration [70, 71]), to colonies of insects [72], to extraordinarily complex systems in vertebrates [73]. A well known example occurring in bacterial motion is that of fingering, which serves as a primary motivation for our mathematical model introduced in this work. Fingering is a motility pattern which is often observed in cell cultures, and is characterized by cellular populations, initially undergoing essentially random and independent motion, forming structured "finger-like" protrusions from their initial homogeneous state [74, 75, 76]. These protrusions indicate the emergence of social hierarchy via "leader-type" cells at the leading edge of the protrusions; the remaining cells "follow" in the paths determined by leading cells, often in very straight lines [76]. Fingering is most closely associated with populations exposed to optical gradients (phototaxis), but is also observed in wound

healing, where cellular communication is determined primarily via chemical (chemotaxis) and mechanical signaling [77, 78, 79, 80]. The formation of leaders/followers is also observed in other biological systems, such as in trail formation and cooperative transport in groups of ants [81, 82, 83, 84] and the marching swarms of locusts as mentioned above [58, 59]. Many biological mechanisms exist by which leader/follower hierarchy emerges, including pheromone signaling [82], slime formation [76], and mechanical pressure [80], although many scientific questions remain [85, 86].

It is the goal of this work to present a minimal mathematical model which describes the emergence of social hierarchy of leaders and followers via pairwise interactions; for a visualization of typical simulations exhibiting line formation, see Figure 2. Our proposed model can be understood from a simple phenomenological perspective: rather than metric-based interaction, $\phi_{ij} = \phi(|\mathbf{x}_i - \mathbf{x}_j|)$, we propose projected-based interactions

$$\phi_{ij} = \phi(\chi_{ij}\mathbf{x}_j - \mathbf{x}_i), \quad \chi_{ij} := \frac{\langle \mathbf{x}_i, \mathbf{x}_j \rangle}{|\mathbf{x}_j|^2}, \quad (8)$$

where the agent positioned at \mathbf{x}_i interacts with the traces of neighboring agents in the forward looking cone $\mathbf{x}_j \in \mathcal{N}_i := \{\beta|\mathbf{x}_i|/|\mathbf{x}_j| \leq \chi_{ij} \leq 1\}$. For a geometric illustration of the projection, see Figure 5. This leads to the spontaneous formation of leaders and followers, defined with respect to relative positions in a linear aggregate. Observe that the interactions in (8) are not symmetric; further, they are not Galilean invariant. Accordingly, there is a need to shift the fixed origin, and trace the dynamics relative to center of mass, $\mathbf{x}_i \mapsto \mathbf{x}_i - \bar{\mathbf{x}}$.

Such interactions can be readily understood in many of the applications described above, such as the sensing of pheromone trails left by neighboring ants, and slime model deposits in

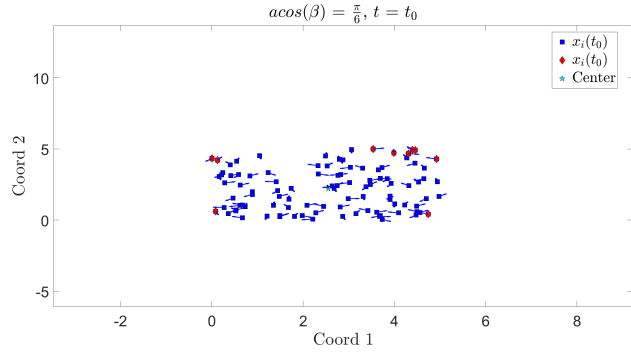


Figure 1: Initial configuration of positions/velocities of second-order system as described in Section 3.2. We simulate $N = 100$ agents (blue squares), with 10 agents (red diamonds) chosen at the initial time as the furthest away from the center of mass (cyan star) at $t_0 = 0$.

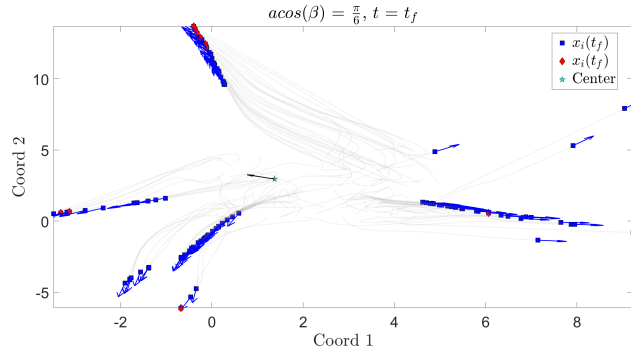


Figure 2: Trajectory plot of second-order system described in Section 3.2 with the initial configuration shown in Figure 1. The coloring of the agents are described in the caption of Figure 1, and the grey trailing lines indicate the path of an agent's trajectory. Note that agents furthest away may not become “leaders.”

bacterial cultures. Although inspired by fingering in phototaxis and chemotaxis, the model assumes no external forcing, so that the emergence of lines is intrinsic to the interactions of the agents alone. Furthermore, the model is sufficiently generic to describe a wide variety of phenomena, including spatial positions and velocity, but also emotions,

frequencies, headings, opinions, etc. as described previously.

The remainder of the paper is organized as follows. We provide a brief discussion of mathematical models of collective motion and chemotaxis/phototaxis in Section 2. In Section 3, we provide a detailed description for the modeling framework, with details of the first- and second-order systems provided in Sections 3.1 and 3.2, respectively. Numerical results for each system are provided in Section 5.1 and Section 5.5, and concluding remarks are provided in Section 6.

2. Alignment models of collective motion and social hierarchy

In this section we restrict our attention to alignment dynamics, suppressing the additional roles of attraction and repulsion. We begin with a brief overview of two alignment models; we refer to [17, 18] for a thorough discussion on the biological phenomena, and to [4] for a recent mathematically rigorous discussion of alignment models.

The first alignment model originates from the 1995 work of Vicsek [14], in which self-propelled particle systems go through local averaging of velocity orientations. Indeed, many physical and biological systems utilize one form or another of environmental averaging [87, 88, 89, 90, 91].

A second velocity alignment model was introduced in 2007 by Cucker and Smale [5, 6]. The model presented in this manuscript is directly inspired by the Cucker-Smale (CS) model, so we describe it in detail here. The system consists of N identical interacting agents, each is identified by its position \mathbf{x}_i and velocity \mathbf{v}_i in \mathbb{R}^d , for

$i = 1, 2, \dots, N$. Their dynamics is governed by

$$\begin{aligned}\dot{\mathbf{x}}_i(t) &= \mathbf{v}_i \\ \dot{\mathbf{v}}_i(t) &= \frac{\tau}{N} \sum_{j=1}^N \phi_{ij}(t)(\mathbf{v}_j(t) - \mathbf{v}_i(t)),\end{aligned}\quad (9)$$

with pairwise interactions driven by $\phi_{ij}(t) = \phi(\mathbf{x}_i(t), \mathbf{x}_j(t))$. The scalar communication kernel, ϕ , quantifies the dynamic influence of agent j on agent i . In the original CS model, the authors advocate the class of long-range, decreasing metric kernels

$$\phi_{ij} = \phi(|\mathbf{x}_i - \mathbf{x}_j|), \quad \phi(r) = \frac{K}{(\alpha^2 + r^2)^\beta}, \quad (10)$$

with constants $K, \beta > 0$. We previously discussed the other classes of singular kernels which emphasize nearby agents over those farther away [11, 12, 13, 92, 93], $\phi(r) = r^{-\beta}$, and the class of short-range kernels, $\phi(r) = \mathbb{1}_{r \leq r_0}$. Metric kernels reflect, by definition, symmetric interactions, $\phi_{ij} = \phi_{ji}$, and we notice that the tacit assumption is that the communication decays with the distance.

Motivated by the original CS model, the general framework of alignment based on pairwise interactions has inspired considerable work, including the hydrodynamic description of its large crowd limit, [9, 94, 95, 2, 96, 97], incorporation of collision avoidance [98], steering [99], and stochasticity [100]. The large-time behavior of CS alignment dynamics (9) should lead the crowd to aggregate into a finite-size cluster, $\max |\mathbf{x}_i(t) - \mathbf{x}_j(t)| \leq D$ which in turn leads to flocking $|\mathbf{x}_i(t) - \mathbf{v}_j(t)| \xrightarrow{t \rightarrow \infty} 0$. However, left without attraction/repulsion, dynamics driven solely by alignment does not support the emergence of any preferred spatial configuration.

As mentioned in Section 1, the goal of this work is to provide a minimal mathematical model which exhibits the emergence of a simple form of social hierarchy through pairwise interactions.

The model is a direct analog of the CS alignment, and is inspired by the biological phenomena of fingering in chemotaxis and phototaxis. It is advocated as a simple alignment mechanism by which a priori identical agents evolve to form fingering structures with internal hierarchy. It should be empathized that there is no attempt to provide our model with external environment which is of course necessary to accurately describe an externally signaled process such as phototaxis/chemotaxis; instead, we limit ourselves to cellular communication mechanisms which, we claim, is an essential part of the more complicated processes. In this sense, this work is complimentary to theoretical and experimental work studying social hierarchy as well as chemotaxis/phototaxis. For example, many works formulate interacting agents systems similar to the Vicsek model [101], which may include an internal excitation variable to model phototaxis both deterministically [102] and stochastically [103, 104, 105]. Slime deposition [106] is also a common mechanism used to describe fingering, with agent-based [30, 107] and continuum partial differential equation [76] proposed. Similar approaches exist in describing chemotaxis, including modeling fingering a free boundary value problem [108], and extensions to the classic chemotaxis equations introduced by Keller and Segel [109, 110, 111]. Hierarchy and leadership has been investigated in the CS model [112] as well as in network graphs with switching topologies [113]. Leadership arising via external signaling was introduced and analyzed in [114], moreover leadership in cells due to feedback in speed and curvature can be formed [115, 116, 117], which we note may be particularly relevant for phototaxis and chemotaxis.

3. Mathematical models of line alignment

Motivated by the discussion in Section 1, we propose both first- and second-order models which describe the emergence of hierarchical structure in interacting agent systems for active particles, which we term generally as “line alignment models.” For both systems, we consider a total of N interacting agents. Each agent is assigned a position $\mathbf{x}_i \in \mathbb{R}^d$, and, in the case of second order models, agents are assigned with additional velocity, $\mathbf{v}_i \in \mathbb{R}^d$. We utilize the projected position, $\chi_{ij}\mathbf{x}_j$, as a way to realize the tendency of agents ‘to look ahead’. In order to avoid the discussion of absolute origin, we also use the center of mass position of the whole system as the reference. We believe this assumption is physically reasonable, as groups of bacteria/cells/animals should not utilize a global coordinate system with specified fixed origin, but rather measure positions with respect to their local environment, e.g. the center of mass of their flock, school, or other social structural unit. Coordinate systems in local environments may be species dependent; for example, bacteria undergoing phototaxis may measure their position relative to a dominant light source [118], while humans in a concert may measure their positions with respect to the main stage. In an isotropic environment, a “natural” coordinate system is the center of mass reference frame. That is, we assume that the interacting agents measure their positions relative to the agent-system itself. For example, we consider the relative positions $\tilde{\mathbf{x}}_i$ and $\tilde{\mathbf{x}}_j$ defined with respect to the center of mass $\bar{\mathbf{x}}$ of the system:

$$\tilde{\mathbf{x}}_i := \mathbf{x}_i - \bar{\mathbf{x}}, \quad \bar{\mathbf{x}}(t) := \frac{1}{N} \sum_{i=1}^N \mathbf{x}_i(t). \quad (11)$$

Here \mathbf{x}_i and \mathbf{x}_j denote the positions of the agents with respect to an arbitrary origin $0 \in \mathbb{R}^d$. For a visualization, see Figure 3. We note that when interactions occur through symmetric

differences of positions, as in the Cucker-Smale and Vicsek models, absolute versus relative positions result in identical dynamical systems, so that the distinction is irrelevant. However, when considering non-symmetric interactions that arise via projected distances as in (8), the resulting systems possess distinct vector fields. Of course, certain species may indeed have global coordinate systems, such as in the mass migration of some species of birds [119].

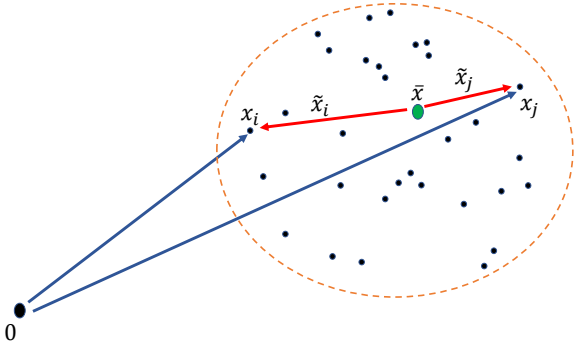


Figure 3: Absolute versus relative position coordinates for agents i and j . Agents are indicated in black, the center of mass of the system $\bar{\mathbf{x}}$ is green, absolute positions are blue, and relative positions (with respect to the center of mass) are red. Positions vectors are indicated for two representative agents only. Note that the center of mass is calculated for the entire N -agent system (see (11)).

3.1. First-order model

We begin by introducing a first-order model, which governs the positions of N interacting agents (cells, birds, humans, etc.). Each agent is described by its time-dependent position $\mathbf{x}_i(t) \in \mathbb{R}^d$. Their dynamics is governed by pairwise interactions,

$$\dot{\mathbf{x}}_i(t) = \frac{1}{|\mathcal{N}_i(t)|} \sum_{j \in \mathcal{N}_i(t)} \phi_{ij}(\chi_{ij} \tilde{\mathbf{x}}_j - \tilde{\mathbf{x}}_i). \quad (12)$$

Here $\phi_{ij}(t)$ quantifies the interactions depending on the projected difference

$$\phi_{ij} := \phi(|\chi_{ij} \tilde{\mathbf{x}}_j - \tilde{\mathbf{x}}_i|), \quad \chi_{ij} := \frac{\langle \tilde{\mathbf{x}}_i, \tilde{\mathbf{x}}_j \rangle}{|\tilde{\mathbf{x}}_j|^2}. \quad (13)$$

Note that in the case that $|\tilde{\mathbf{x}}_j| = 0$ (i.e. agent j is located at the center of mass of the system), the projection χ_{ij} is defined as zero. The neighborhood of agent positioned at \mathbf{x}_i is formed via a *forward cone*, which models the asymmetric phenomenon of “looking ahead”,

$$\mathcal{N}_i := \{j \mid \beta |\tilde{\mathbf{x}}_i| |\tilde{\mathbf{x}}_j| \leq \langle \tilde{\mathbf{x}}_i, \tilde{\mathbf{x}}_j \rangle \leq |\tilde{\mathbf{x}}_j|^2\}, \quad (14)$$

where $0 < \beta \leq 1$ is a fixed constant which determines the angular size of the forward cones[‡]. As before, $\phi(\cdot)$ is a communication kernel which quantifies the dynamic influence of the traced agent j on agent positioned at \mathbf{x}_i . In this work, we limit ourselves to metric communication kernels.

To model line alignment, we specify both — the pairwise interaction of agents at distance $r_{ij} = |\chi_{ij} \tilde{\mathbf{x}}_j - \tilde{\mathbf{x}}_i|$, as well as the spatial neighborhoods defining which agents influence the dynamics of one another. The spatial neighborhoods are necessarily non-symmetric, but rather “forward-facing”; for example, if the agent positioned at \mathbf{x}_i is positioned ahead and “in view” of the agent positioned at \mathbf{x}_j , then agent j should be influenced by agent i , but not vice versa. The notions of positioned ahead and in view of are quantified via \mathcal{N}_i — the neighborhood of agent i , i.e. the set of agents which influence the dynamics of agent i .

Note that we use relative coordinates $\tilde{\mathbf{x}}_i$ and $\tilde{\mathbf{x}}_j$ to determine the forward cone, based at the corresponding center of mass $\bar{\mathbf{x}}$. Each cone is defined via a central angle of $2 \cos^{-1}(\beta)$ radians, which is symmetric about the $\tilde{\mathbf{x}}_i$ direction; this is the left-hand inequality in (14). The right-hand inequality ensures that agents are only

[‡] For simplicity, we assume the opening of forward looking cones to be the same for all agents.

influenced by other agents in front of them in relative position space, so that the cone is indeed forward-facing. The latter can be understood by noting that the right-hand inequality in (14) restricts the length of the projection of $\tilde{\mathbf{x}}_i$ along $\tilde{\mathbf{x}}_j$, i.e. $|\tilde{\mathbf{x}}_i| \cos(\phi) \leq |\tilde{\mathbf{x}}_j|$ where ϕ is the angle between $\tilde{\mathbf{x}}_i$ and $\tilde{\mathbf{x}}_j$, so that we require $\tilde{\mathbf{x}}_j$ to be ahead of $\tilde{\mathbf{x}}_i$ in relation to $\bar{\mathbf{x}}$. Since all positions $\tilde{\mathbf{x}}_i$ are time-varying, each \mathcal{N}_i changes in time t ; a static visualization of the conic spatial region is provided in Figure 4. Geometrically, the influence of agent j on its

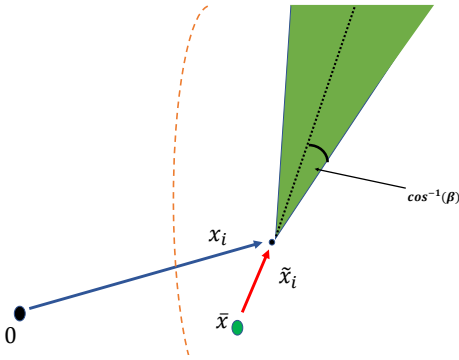


Figure 4: Forward cone defining a neighborhood \mathcal{N}_i for agent i in system (12). The green forward conic region indicates the spatial region defining \mathcal{N}_i in (14). Note that all positions depend on time t , so that conic region moves with the agents in time.

dynamics, agent i measures its difference in projected position relative to agent j . Thus, the form of (12) tends to align agents along lines, as the pairwise interactions ‘aim’ to reduce the orthogonal distance between agents i and j . As ϕ is tacitly assumed to be decreasing, agents are more influenced by their nearer neighbors inside the forward-looking cone, i.e. with those that are more aligned with their current direction. A visualization is provided in Figure 5. To completely specify the dynamics, a set of initial conditions $\{\mathbf{x}_i(0)\}_{i=1}^N$ must also be prescribed. Details on initial conditions and other parameters

investigated are provided in Section 5.1.

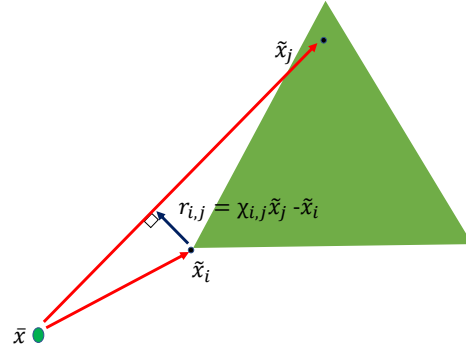


Figure 5: Difference vector \mathbf{r}_{ij} measuring the difference between $\tilde{\mathbf{x}}_i$ and its projection along $\tilde{\mathbf{x}}_j$. Vector \mathbf{r}_{ij} measures how aligned agent i is with respect to agent j . Line alignment implies that agent i acts to reduce \mathbf{r}_{ij} for all agents j in its forward cone.

3.2. Second-order model

We can now introduce the second-order model, analogous to the first-order model detailed in Section 3.1, but in which pairwise interactions influence the *acceleration* of the agents; this is in contrast with (12), where agents directly regulate velocity. This framework is more closely related to a classical mechanics perspective, where the interaction terms are precisely interaction *forces*. The state-space is represented by the position and velocity vectors of the N agents, i.e. $\{\mathbf{x}_i, \mathbf{v}_i\}_{i=1}^N$, where the second-order dynamics reads

$$\begin{aligned} \dot{\mathbf{x}}_i(t) &= \mathbf{v}_i(t) \\ \dot{\mathbf{v}}_i(t) &= \frac{1}{|\mathcal{N}_i(t)|} \sum_{j \in \mathcal{N}_i(t)} \left(\phi(|\mathbf{r}_{ij}(t)|) \mathbf{r}_{ij}(t) \right. \\ &\quad \left. + \psi(|\mathbf{r}_{ij}(t)|) (\mathbf{v}_j(t) - \mathbf{v}_i(t)) \right) \end{aligned} \quad (15)$$

Here $\mathbf{r}_{ij} := \chi_{ij} \tilde{\mathbf{x}}_j - \tilde{\mathbf{x}}_i$ denotes the orthogonal component of $\tilde{\mathbf{x}}_i$ projected in the direction of $\tilde{\mathbf{x}}_j$, so that agents interact via relative projected directions as discussed in Section 3.1 (see

equation (13)), and hence act to align “along lines”. The functions ϕ and ψ characterize the strength of the interactions, both depend on the projected distances, $r_{ij} = |\mathbf{r}_{ij}|$, between agent currently positioned at $\tilde{\mathbf{x}}_i$, and the agent currently positioned at $\tilde{\mathbf{x}}_j$ which is traced to its backward position $\chi_{ij}\tilde{\mathbf{x}}_j$. Interactions are again local, and the net effect on the dynamics of agent i is the superposition of the interaction forces from all “forward-looking” neighboring agents $j \in \mathcal{N}_i$.

The pairwise interactions are determined by the two function ϕ and ψ . We first observe that force governed by ϕ is identical to that of the first-order attraction/repulsion in (4). The second term, dictated by interaction kernel ψ , is an extension of the Cucker-Smale velocity alignment force [5, 6]. The velocity alignment in our second-order model ensures that in equilibrium, the emergent “finger-like” lines lead to flocking, $|\mathbf{v}_i(t) - \mathbf{v}_j(t)| \xrightarrow{t \rightarrow \infty} 0$. Indeed, the line formation will stay stable only when all the agents are moving with the same velocity; otherwise the lines formed will not be stable.

4. From alignment to the emergence of lines

The key feature of the first- and second-order models, (12), and respectively, (15), is the emergence of geometric structure for the trails along which the crowd is aligned — specifically, we observe the large-time formation of curves turning into straight lines; consult the numerical simulations reported in Section 5 below. A detailed analysis of this phenomenon is beyond the scope of this work and will be provided in a future work. Here we quote a prototypical result. We consider the first-order line alignment model

$$\begin{aligned} \dot{\mathbf{x}}_i(t) &= \frac{\tau}{\sigma_i} \sum_{j \in \mathcal{N}_i(t)} \phi_{ij} (\chi_{ij} \mathbf{x}_j(t) - \mathbf{x}_i(t)), \\ \chi_{ij} &= \frac{\langle \mathbf{x}_i, \mathbf{x}_j \rangle}{|\mathbf{x}_j|^2}, \quad \sigma_i := \sum_{j \in \mathcal{N}_i} \phi_{ij}. \end{aligned} \quad (16)$$

To simplify our discussion, we set the dynamics relative to a fixed origin, so that $\tilde{\mathbf{x}}_i \mapsto \mathbf{x}_i$. The specifics of the projected-based communication, given by $\phi_{ij} = \phi(\chi_{ij} \mathbf{x}_j - \mathbf{x}_i)$, are not essential; indeed it is remarkable that our results apply to a wide variety of communication protocols, independent of symmetry or occupying a global stencil. Here, we use an adaptive normalization of the communication protocol as in [34], replacing $N_i \mapsto \sigma_i$, so that $\frac{1}{\sigma_i} \sum_{j \in \mathcal{N}_i} \phi_{ij} = 1$ (so that the dynamics does not involve ‘counting’ the number of agents).

THEOREM 1. *Consider the line alignment model (16), dictated by a decreasing kernel $\phi(r)$, which acts inside the forward-looking cones*

$$\mathcal{N}_i := \{j \mid \beta |\mathbf{x}_i| |\mathbf{x}_j| \leq \langle \mathbf{x}_i, \mathbf{x}_j \rangle \leq |\mathbf{x}_j|^2\}, \quad \beta > 0.$$

Then, there exist constants, C_0 depending on the initial configuration and C_ϕ depending on ϕ , such that the following holds,

$$\begin{aligned} \sum_i \sum_{j \in \mathcal{N}_i} \left(|\mathbf{x}_i(t)|^2 \cdot |\mathbf{x}_j(t)|^2 \right. \\ \left. - |\langle \mathbf{x}_i(t), \mathbf{x}_j(t) \rangle|^2 \right) \leq C_0 e^{-C_\phi \beta^2 t}. \end{aligned}$$

Theorem 1 precisely quantifies the emergence phenomenon in the first-order model (12). Namely — the crowd forms one or more distinct straight trails, led by an agent \mathbf{x}_i and followed by its neighbors $\{\mathbf{x}_j, j \in \mathcal{N}_i\}$ so that $|\mathbf{x}_i| \cdot |\mathbf{x}_j| - \langle \mathbf{x}_i, \mathbf{x}_j \rangle \xrightarrow{t \rightarrow \infty} 0$. The remarkable aspect of the line dynamics, reflected in Theorem 1, is that the ‘kinetic energy’, $\sum_i \sum_{j \in \mathcal{N}_i} |\mathbf{x}_i(t)|^2 \cdot |\mathbf{x}_j(t)|^2$ is easily shown to be decreasing in time. The ‘potential energy’, however, $\sum_i \sum_{j \in \mathcal{N}_i} |\langle \mathbf{x}_i(t), \mathbf{x}_j(t) \rangle|^2$, does not exhibit a time-monotone behavior and may change with the configuration. It is their difference that is decreasing in time, reflecting the emergent behavior. To our knowledge, it is the first large-time, large-crowd emergence dynamics based on local interactions (the neighborhoods \mathcal{N}_i ’s).

5. Numerical results

In this section, we numerically investigate the models of social hierarchy presented in Section 3. Specifically, we demonstrate the emergence of lines in both the first- and second-order models, and study the effect of model parameters, including the number of agents and type of interaction kernel, on the resulting dynamics. We also show that the formation of leader agent is indeed emergent, and cannot be easily extrapolated via initial conditions alone.

5.1. First-order model line formation

We begin by simulating the first-order line alignment model(12) with parameters appearing in Table 1. We are thus simulating $N = 100$ agents over a period of 50 time units in a two spatial dimensions. Here μ_0 denotes a probability distribution utilized for generating the initial positions, with $\mathcal{U}([0, 5]^2)$ representing the uniform distribution over $[0, 5]^2$. Thus, we assume that the agents are initially uniformly distributed over a square region in the plane. A fixed realization of initial positions of agents is used for all simulations in this subsection, which is provided in Figure 6. In this subsection, we assume a topological interaction kernel as discussed in Section 1:

$$\phi(r) = \mathbb{1}_{r \leq 1}(r) \quad \text{or} \quad (17)$$

$$\phi(r) = \frac{1}{(1 + r^2)^{0.25}}, \quad (18)$$

where r denotes the projected difference between agents with respect to an agent's forward cone (see equation (13)). Recall that $\mathbb{1}_{r \leq 1}$ denotes the indicator function on the set $[0, 1]$, so that all agents with projected distance less than one unit inside of the forward cone equally influence the dynamics of the agent. All simulations, in this and other sections, are integrated using

MATLAB's built-in adaptive integrator ode23 for handling possible stiffness of the system.

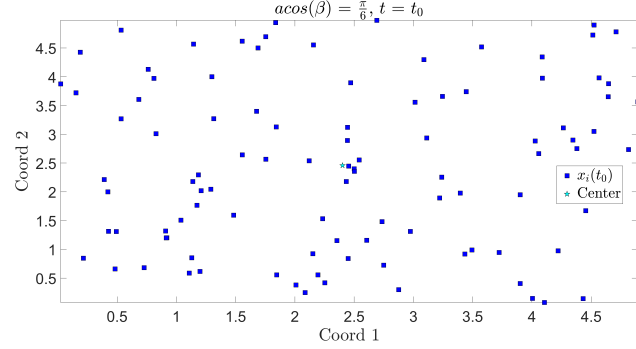


Figure 6: Initial configuration of positions for $N = 100$ agents for first-order system with parameters as in Table 1.

μ_0	d	N	t_0	t_f
$\mathcal{U}([0, 5]^2)$	2	100	0	50

Table 1: Parameters utilized to simulate the first-order model as discussed in Section 5.1.

We begin by demonstrating that the proposed first-order model asymptotically exhibits line formation. Consider Figure 7, which assumes a forward cone with central angle $\pi/3$ and interaction kernel given by (17). Blue squares in the figure represent agent positions $\mathbf{x}_i(t)$ and the cyan star represents the center of mass position of the system, i.e. $\bar{\mathbf{x}}_i(t)$. Recall that the center of mass is not stationary, and that all agent measure relative coordinates with respect to $\bar{\mathbf{x}}_i(t)$. In this figure, we clearly observe the formation of spatial lines which originate from center of mass of the system. This hierarchical structure emerges from the initial uniform distribution of positions in Figure 6, and hence can be thought of as a form of emergence of social hierarchy. Note that the “leaders” here correspond to the agents farthest from the center of mass of the system. The dynamics thus represent a rudimentary form of finger

morphology as discussed in Section 1.2, which occurs through purely inter-agent interactions, with no reliance on external forces. It may appear that the leader's form from those agents initially farthest from the center of mass of the system, but this is not necessarily true; see Section 5.6 for details regarding the second-order model. We also emphasize that the system has reached equilibrium, as simulating further in time (not shown) produces the same spatial pattern observed in Figure 7.

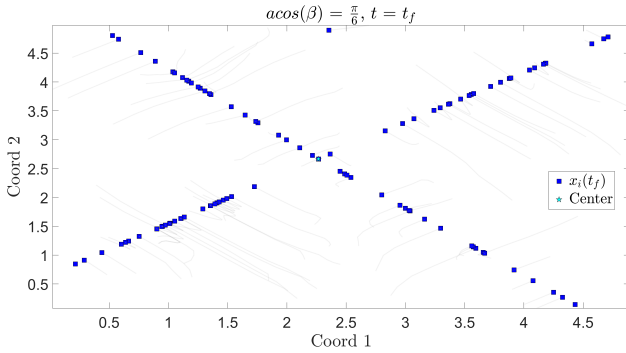


Figure 7: Trajectory plot for the first order system with parameters taken from table 1 with $\beta = \frac{\pi}{6}$ and $\phi = \mathbb{1}_{r \leq 1}$, the initial configuration of positions is shown Figure 6. We clearly observe the formation of lines.

5.2. Variation of dynamics as a function of forward cone size

We investigate the dynamics of line formation as a function of the size of the forward cone. Specifically, we are interested in understanding the effect of the angular size of the cone, defined by β (see Figure 4), on the dynamics line formation. Questions of specific interest are both the the number and density of lines formed, which thus correspond to the number of emergent leaders (equivalently, the number of “fingers” formed). Intuitively, we expect that the number of lines formed should increase as the size of the forward cone decreases, as each

agent acts with a higher degree of locality. For a demonstration, see Figure 8, which utilizes the same initial conditions and parameters as in Figure 7, with the exception that a central angle corresponding to π defines the forward cone (note that in the case, it is really a forward *plane*, and not a cone). We observe a similar pattern of lines compared to the smaller, and hence more local, forward cone, but with a significantly higher degree of clustering to points, so that the asymptotic behavior is more similar to *points*, as opposed to lines. The mechanisms that produces this behavior is due to a combination of two factors: 1) the dynamics are first-order, and hence tend to exhibit aggregation, and 2) the interaction kernel (17) assumes a uniformity of influence with respect to all neighboring agents. To see the resulting pattern formation, and the effect of varying β , for the CS interaction kernel (18), see Section 5.4.

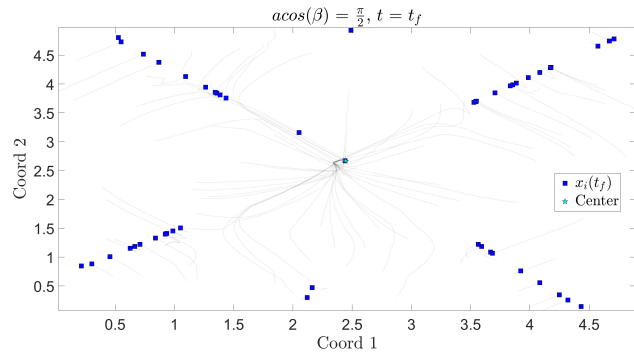


Figure 8: Trajectory plot for the first-order system with parameters taken from Table 1 with $\beta = \frac{\pi}{2}$ and $\phi = \mathbb{1}_{r \leq 1}$, and initial configuration of positions is shown in Figure 6. We clearly observe the formation of lines, with significant clustering about the center of mass (compare to Figure 7).

5.3. Variation of dynamics as a function of initial conditions

In the previous section, we studied line formation for a fixed set of initial conditions. Also of interest is the role of initial conditions on the distribution of lines. More precisely: is the resulting pattern robust or highly sensitive to the agent's initial positions? Numerical simulations (not provided) suggest that the final configuration of lines (both number of lines, and orientations) are highly dependent on the initial conditions; resampling μ_0 generally results in a different equilibrium distribution. We note that this is not surprising, and it is common feature of models describing collective motion. Similarly, we investigate how the behavior changes as a function of number of agents (N in Table 1). This a natural scientific question, as line formation occurs across a variety of scales; for example, the number of ants composing a trail be on the order of one hundred, while the number of bacteria generating finger morphology in phototaxis may be on the order of one thousand. Furthermore, such questions are of mathematical interest, as they may provide insight into corresponding coarse-grained macroscopic models, such as mean-field and hydrodynamic limits, described by Boltzmann-type partial differential equations. We thus investigate to what degree the social hierarchy model proposed in this work is dependent on the number of agents in the system. As an example, we repeat simulations appearing in Figures 7 and 8, with fewer agents ($N = 50$ versus $N = 100$ previously; new initial conditions are provided in Figure 9); corresponding results can be found in Figures 10 and 11. Similar qualitative dynamics are apparent for the smaller system, but in general we see that the distributions of lines is quite different, even for the corresponding forward cones.

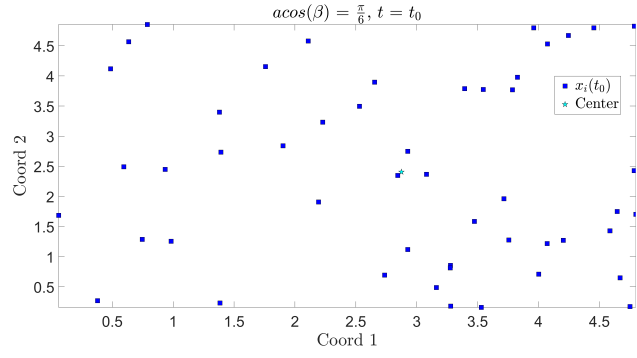


Figure 9: Initial configuration of position for first-order system with the parameters taken from Table 1, except for a smaller number of agents ($N = 50$).

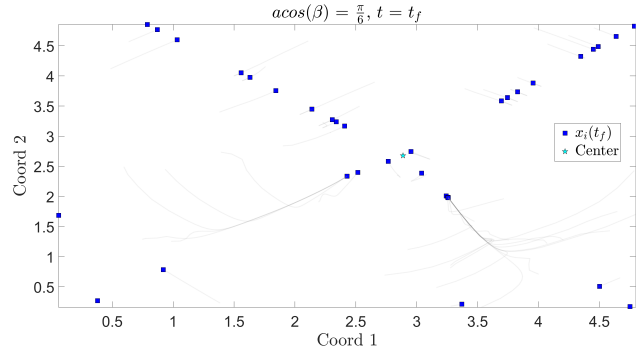


Figure 10: Trajectory plot for the first-order system with parameters taken from Table 1 with $\beta = \frac{\pi}{6}$ and $\phi = \mathbb{1}_{r \leq 1}$, and initial configuration of positions is shown in Figure 9.

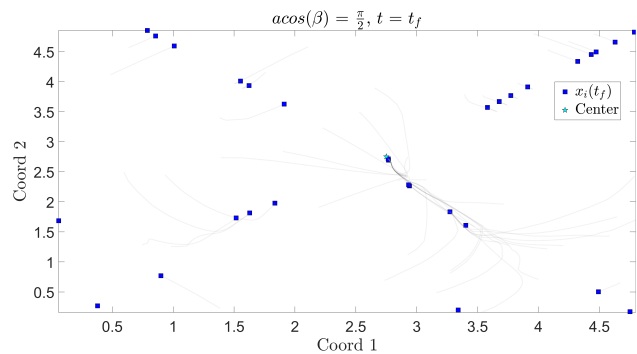


Figure 11: Trajectory plot for the first-order system with parameters taken from table 1 with $\beta = \frac{\pi}{2}$ and $\phi = \mathbb{1}_{r \leq 1}$, and initial configuration of positions is shown in Figure 9.

5.4. Effect of interaction function on pattern formation

In the previous sections, we assumed a topological interaction kernel given by (17), which weights all neighboring agents equally in a forward cone with a limited support. We here instead use a global interaction function, i.e. $\phi = \frac{1}{(1+r^2)^{0.25}}$, to demonstrate the effect of the interaction function on line formation for two different β values. As discussed in Section 5.2, we expect a global kernel to exhibit a more pronounced response to the forward cone size with respect to angle β . Results of simulations are provided in Figures 12 and 13. Compared to the locally supported ϕ (Figures 7 and 8), this system's final distribution of lines shows considerable variation: two lines for $\beta = \pi/6$ become one for $\beta = \pi/2$. Note that the initial configuration of position is the same as shown in Figure 6.

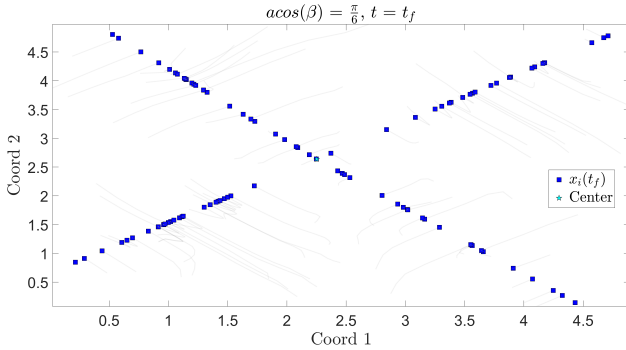


Figure 12: Trajectory plot for the first-order system with parameters taken from Table 1 with $\beta = \frac{\pi}{6}$ and $\phi = \frac{1}{(1+r^2)^{0.25}}$, and initial configuration of positions is shown in Figure 6.

5.5. Second-order model simulation results

We next simulate the second-order model (15) to demonstrate the dynamics of line formation in a system where interactions affect acceleration; simulation details are provided in Table 2. Recall from Section 3.2 that we must specify two

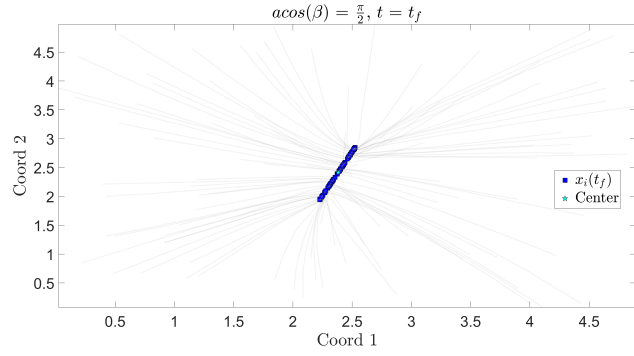


Figure 13: Trajectory plot for the first-order system with parameters taken from Table 1 with $\beta = \frac{\pi}{2}$ and $\phi = \frac{1}{(1+r^2)^{0.25}}$, and initial configuration of positions is shown in Figure 6.

interaction kernels: ϕ , which governs the inter-agent interaction force of line alignment, and ψ , which accounts for velocity alignment and hence stabilization. Note that ϕ is completely analogous to the first-order model, except it more directly corresponds to a classical Newtonian force law, as the system is second-order. We assume the same function dependence (17) for ϕ , and assume the classical Cucker-Smale interaction kernel for ψ :

$$\psi(r) = \frac{1}{(1+r^2)^{1/2}}. \quad (19)$$

μ_0^x	μ_0^y	d	N	t_0	t_f	ϕ	ψ
$[0, 5]^2$	\mathbb{B}^2	2	100	0	10	$\mathbb{1}_{r \leq 1}$	$\frac{1}{(1+r^2)^{1/2}}$

Table 2: Parameters utilized to simulate the second-order model as discussed in Section 5.5.

Here \mathbb{B}^2 is the $2D$ unit ball centered at the origin. We simulate the models for different values of β to investigate the effect of the various sizes of the neighborhood, as in Section 5.2 for the first-order model. All tests use the same initial condition, with the initial position $\mathbf{x}_i(t_0)$ being an independent and identically distributed (i.i.d) sample from μ_0^x , and the initial velocity being an i.i.d sample from

μ_0^v . Figure 14 provides the realization of the initial configuration of positions/velocities for all the tests of different β values investigated in this work. The blue dots in the figures represent the position (i.e. $x_i(t)$) of the agents with the yellow arrow representing the velocity (i.e. $v_i(t)$), whereas the cyan dot represents the center of mass position, and $\bar{x}_i(t)$ with the yellow arrow representing the center of mass velocity $\bar{v}_i(t)$. Results are provided in Figures 15-19, where we have again considered variation in forward cone size (β) and number of agents ($N = 100$ versus $N = 50$). The results are qualitatively similar to the first-order system, although the second-order system exhibits a much richer class of dynamics, as the system does not approach equilibrium configurations (this is because inter-agent forces act on accelerations and not velocities, i.e. the system is not dissipative). Note that local groups of agents initially form curved lines of hierarchy (“leaders-followers”) which eventually straighten due to the projected interaction kernel (Figure 2). It thus appears that the competition between line formation (induced by ϕ_1) and flocking (induced by ϕ_2) has made the emergent pattern more interesting. As shown in three of the four examples of different β (with larger β), the system as a whole can produce different flocking velocities, yet social hierarchy (in this case, lines) can emerge from the initially chaotic configuration.

5.6. Initial conditions are not simple predictors of leader emergence

We note that the emergence of leaders is not a simple function of initial distance from the initial center of mass, and thus hierarchy is indeed emergent from the proposed inter-agent dynamics. Consider Figure 2, which shows a number of flocking lines (“fingers”) emerging from an initially random distribution of positions

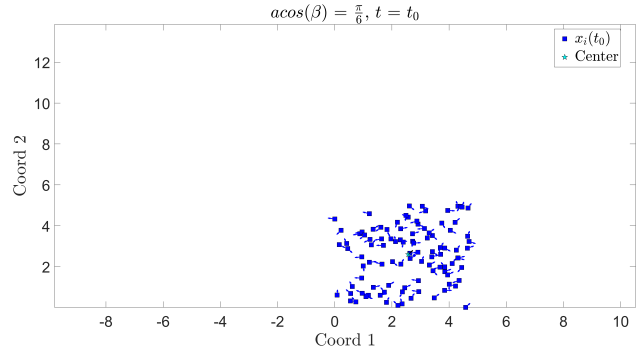


Figure 14: Initial configuration of positions and velocities for second-order system of $N = 100$ agents with the parameters taken from Table 2.

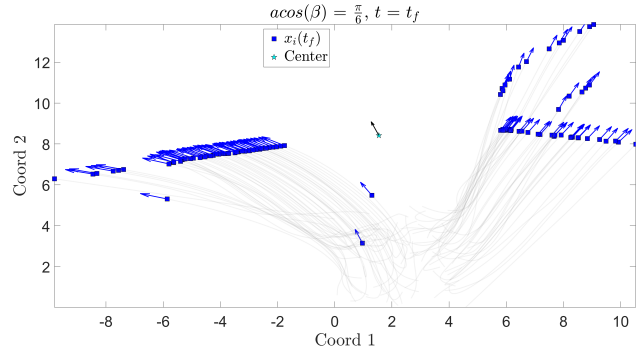


Figure 15: Trajectory plot for the second-order system with parameters taken from Table 2 with $\beta = \frac{\pi}{6}$, and initial configuration of positions/velocities is shown in Figure 14.

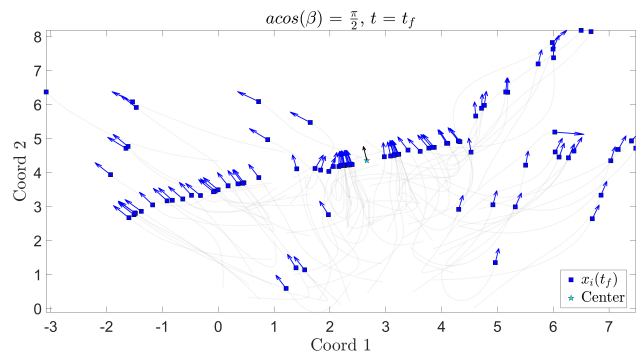


Figure 16: Trajectory plot for the second-order system with parameters taken from Table 2 with $\beta = \frac{\pi}{2}$, and initial configuration of positions/velocities is shown in Figure 14.

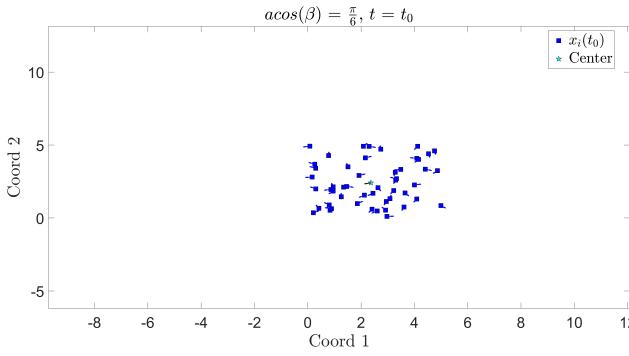


Figure 17: Initial configuration of position for second-order system with the parameters taken from Table 2 for two different β values and $N = 50$.

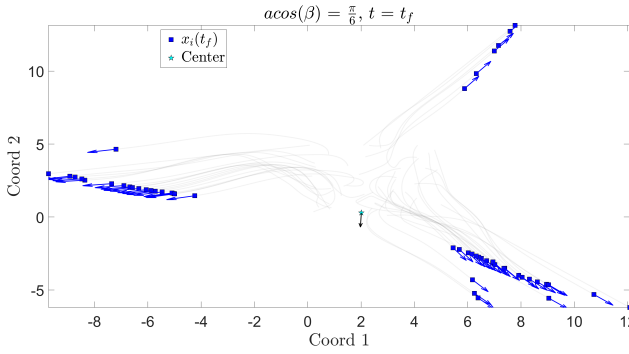


Figure 18: Trajectory plot for the second-order system with parameters taken from Table 2 with $\beta = \frac{\pi}{6}$, and initial configuration of positions/velocities is shown in Figure 17.

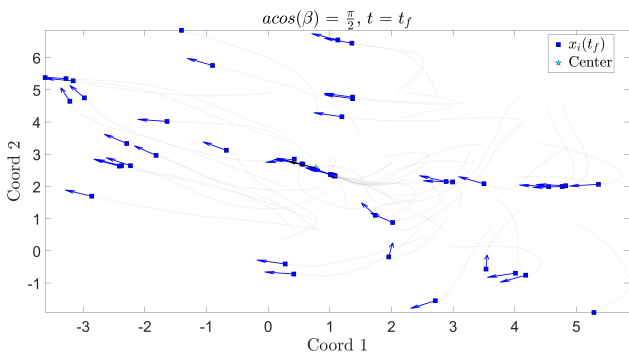


Figure 19: Trajectory plot for the second-order system with parameters taken from Table 2 with $\beta = \frac{\pi}{2}$, and initial configuration of positions/velocities is shown in Figure 17.

and velocities (Figure 14). In Figure 2, we have colored red the 10 initial agents farthest from the initial center of mass. Note that some agents that were initially farthest from the center of mass become followers; for example, in the right-hand side, there is a line of agents with an initially distant agent (red) that becomes a “follower.” Similarly, we see that some agents that were initially near the center of mass become “leaders” of groups of agents. Hence, we see that the model does indeed exhibit emergence of social hierarchy.

6. Discussion and conclusions

In this work, we have presented two collective dynamic models, namely a first-order and a second-order systems, where the emergence of social hierarchy, aka line formation, is induced from the “looking ahead” tendency of agents. These two models are minimal in a sense that the “look-ahead” tendency is implemented using a projected distance together with a forward-cone neighborhood. These models show promising features of natural emergence of geometric structures for various different kinds of initial configurations. More complicated patterns can be induced by using different types of communication kernels (ϕ or ψ). We have presented numerous numerical simulations, and are currently developing a mathematical theory to rigorously understand properties of the emergence of line formation in such models. .

- [1] Julia K Parrish and William M Hamner. Animal groups in three dimensions: how species aggregate. Cambridge University Press, 1997.
- [2] Sebastien Motsch and Eitan Tadmor. Heterophilous dynamics enhances consensus. SIAM review, 56(4):577–621, 2014.
- [3] Roman Shvydkoy et al. Dynamics and analysis of alignment models of collective behavior. Springer, 2021.
- [4] Eitan Tadmor. On the mathematics of swarming: emergent behavior in alignment dynamics. Notices of the AMS, 68:493–503, 2021.
- [5] Felipe Cucker and Steve Smale. Emergent behavior in flocks. IEEE Transactions on automatic control, 52(5):852–862, 2007.
- [6] Felipe Cucker and Steve Smale. On the mathematics of emergence. Japanese Journal of Mathematics, 2(1):197–227, 2007.
- [7] Michele Ballerini, Nicola Cabibbo, Raphael Candelier, Andrea Cavagna, Evaristo Cisbani, Irene Giardina, Vivien Lecomte, Alberto Orlandi, Giorgio Parisi, Andrea Procaccini, et al. Interaction ruling animal collective behavior depends on topological rather than metric distance: Evidence from a field study. Proceedings of the national academy of sciences, 105(4):1232–1237, 2008.
- [8] Roman Shvydkoy and Eitan Tadmor. Topologically based fractional diffusion and emergent dynamics with short-range interactions. SIAM Journal on Mathematical Analysis, 52(6):5792–5839, 2020.
- [9] SY Ha and E Tadmor. From particle to kinetic and hydrodynamic descriptions of flocking. Kinetic and Related Models, 1(3):415–435, 2008.
- [10] S.Y. Ha and J.G. Liu. A simple proof of the cucker-smale flocking dynamics and mean-field limit. Commun. Math. Sci., 7:297–325, 2009.
- [11] Jan Peszek. Discrete cucker-smale flocking model with a weakly singular weight. SIAM Journal on Mathematical Analysis, 47(5):3671–3686, 2015.
- [12] Roman Shvydkoy and Eitan Tadmor. Eulerian dynamics with a commutator forcing. Transactions of Mathematics and its Applications, 1(1), 2017.
- [13] Tam Do, Alexander Kiselev, Lenya Ryzhik, and Changhui Tan. Global regularity for the fractional euler alignment system. Archive for Rational Mechanics and Analysis, 228:1–37, 2018.
- [14] Tamás Vicsek, András Czirók, Eshel Ben-Jacob, Inon Cohen, and Ofer Shochet. Novel type of phase transition in a system of self-driven particles. Physical review letters, 75(6):1226, 1995.
- [15] Ruiwen Shu and Eitan Tadmor. Flocking hydrodynamics with external potentials. Archive for Rational Mechanics and Analysis, 238:347–381, 2020.
- [16] Craig W Reynolds. Flocks, herds and schools: A distributed behavioral model. In Proceedings of the 14th annual conference on Computer graphics and interactive techniques, pages 25–34, 1987.
- [17] Tamás Vicsek and Anna Zafeiris. Collective motion. Physics reports, 517(3-4):71–140, 2012.
- [18] M Cristina Marchetti, Jean-François Joanny, Sriram Ramaswamy, Tanniemola B Liverpool, Jacques Prost, Madan Rao, and R Aditi Simha. Hydrodynamics of soft active matter. Reviews of modern physics, 85(3):1143, 2013.
- [19] François Graner and Daniel Riveline. ‘the forms of tissues, or cell-aggregates’: D’arcy thompson’s influence and its limits. Development, 144(23):4226–4237, 2017.
- [20] Taro Toyoda, Shin-Ichi Mae, Hiromi Tanaka, Yasushi Kondo, Michinori Funato, Yoshiya Hosokawa, Tomomi Sudo, Yoshiya Kawaguchi, and Kenji Osafune. Cell aggregation optimizes the differentiation of human escs and ipscs into pancreatic bud-like progenitor cells. Stem cell research, 14(2):185–197, 2015.
- [21] Xing Zhang, Li-hua Xu, and Qiang Yu. Cell aggregation induces phosphorylation of pcam-1 and pyk2 and promotes tumor cell anchorage-independent growth. Molecular cancer, 9(1):1–11, 2010.
- [22] Zahia Bayoussef, James E Dixon, Snjezana Stolnik, and Kevin M Shakesheff. Aggregation promotes cell viability, proliferation, and differentiation in an in vitro model of injection cell therapy. Journal of tissue engineering and regenerative medicine, 6(10):e61–e73, 2012.
- [23] Karine Glinel, Pascal Thebault, Vincent Humblot, Claire-Marie Pradier, and Thierry Jouenne. Antibacterial surfaces developed from bio-inspired approaches. Acta biomaterialia, 8(5):1670–1684, 2012.
- [24] Shane K Green, Andrea Frankel, and Robert S Kerbel. Adhesion-dependent multicellular drug resistance. Anti-cancer drug design, 14(2):153–168, 1999.
- [25] Brad St Croix and Robert S Kerbel. Cell adhesion and drug resistance in cancer. Current opinion in oncology, 9(6):549–556, 1997.
- [26] Joel S Brown, Jessica J Cunningham, and Robert A Gatenby. Aggregation effects and population-

- based dynamics as a source of therapy resistance in cancer. *IEEE Transactions on Biomedical Engineering*, 64(3):512–518, 2016.
- [27] Orit Lavi, James M Greene, Doron Levy, and Michael M Gottesman. The role of cell density and intratumoral heterogeneity in multidrug resistance modeling the intratumoral heterogeneity in multidrug resistance. *Cancer research*, 73(24):7168–7175, 2013.
- [28] Peter Friedl and Darren Gilmour. Collective cell migration in morphogenesis, regeneration and cancer. *Nature reviews Molecular cell biology*, 10(7):445–457, 2009.
- [29] Eric Theveneau and Roberto Mayor. Neural crest migration: interplay between chemorepellents, chemoattractants, contact inhibition, epithelial–mesenchymal transition, and collective cell migration. *Wiley Interdisciplinary Reviews: Developmental Biology*, 1(3):435–445, 2012.
- [30] P Varuni, Shakti N Menon, and Gautam I Menon. Phototaxis as a collective phenomenon in cyanobacterial colonies. *Scientific reports*, 7(1):1–10, 2017.
- [31] Lesley J Morrell and Richard James. Mechanisms for aggregation in animals: rule success depends on ecological variables. *Behavioral Ecology*, 19(1):193–201, 2008.
- [32] Iain D Couzin, Jens Krause, Richard James, Graeme D Ruxton, and Nigel R Franks. Collective memory and spatial sorting in animal groups. *Journal of theoretical biology*, 218(1):1–11, 2002.
- [33] Iain D Couzin and Nigel R Franks. Self-organized lane formation and optimized traffic flow in army ants. *Proceedings of the Royal Society of London. Series B: Biological Sciences*, 270(1511):139–146, 2003.
- [34] Sebastien Motsch and Eitan Tadmor. A new model for self-organized dynamics and its flocking behavior. *Journal of Statistical Physics*, 144(5):923–947, 2011.
- [35] Larissa Conradt and Timothy J Roper. Consensus decision making in animals. *Trends in ecology & evolution*, 20(8):449–456, 2005.
- [36] Jens Krause, Daniel J Hoare, Darren Croft, James Lawrence, Ashley Ward, Graeme D Ruxton, Jean-Guy J Godin, and Richard James. Fish shoal composition: mechanisms and constraints. *Proceedings of the Royal Society of London. Series B: Biological Sciences*, 267(1456):2011–2017, 2000.
- [37] CK Hemelrijk, DAP Reid, H Hildenbrandt, and JT Padding. The increased efficiency of fish swimming in a school. *Fish and Fisheries*, 16(3):511–521, 2015.
- [38] Stefano Marras, Shaun S Killen, Jan Lindström, David J McKenzie, John F Steffensen, and Paolo Domenici. Fish swimming in schools save energy regardless of their spatial position. *Behavioral ecology and sociobiology*, 69(2):219–226, 2015.
- [39] Andrea Cavagna, Irene Giardina, Alberto Orlandi, Giorgio Parisi, Andrea Procaccini, Massimiliano Viale, and Vladimir Zdravkovic. The starflag handbook on collective animal behaviour: Part i, empirical methods. *arXiv preprint arXiv:0802.1668*, 2008.
- [40] Michele Ballerini, Nicola Cabibbo, Raphael Candelier, Andrea Cavagna, Evaristo Cisbani, Irene Giardina, Alberto Orlandi, Giorgio Parisi, Andrea Procaccini, Massimiliano Viale, et al. Empirical investigation of starling flocks: a benchmark study in collective animal behaviour. *Animal behaviour*, 76(1):201–215, 2008.
- [41] Iztok Lebar Bajec and Frank H Heppner. Organized flight in birds. *Animal Behaviour*, 78(4):777–789, 2009.
- [42] Hangjian Ling, Guillam E McIvor, Kasper van der Vaart, Richard T Vaughan, Alex Thornton, and Nicholas T Ouellette. Local interactions and their group-level consequences in flocking jackdaws. *Proceedings of the Royal Society B*, 286(1906):20190865, 2019.
- [43] Lacey F Hughey, Andrew M Hein, Ariana Strandburg-Peshkin, and Frants H Jensen. Challenges and solutions for studying collective animal behaviour in the wild. *Philosophical Transactions of the Royal Society B: Biological Sciences*, 373(1746):20170005, 2018.
- [44] Anne E Goodenough, Natasha Little, William S Carpenter, and Adam G Hart. Birds of a feather flock together: Insights into starling murmuration behaviour revealed using citizen science. *PloS one*, 12(6):e0179277, 2017.
- [45] Thomas Mueller, Robert B O’Hara, Sarah J Converse, Richard P Urbanek, and William F Fagan. Social learning of migratory performance. *Science*, 341(6149):999–1002, 2013.
- [46] Lauren V Ritters, Cynthia A Kelm-Nelson, and Jeremy A Spool. Why do birds flock? a role for opioids in the reinforcement of gregarious social interactions. *Frontiers in Physiology*, 10:421, 2019.
- [47] Raphaël Sarfati, Julie C Hayes, and Orit Peleg. Self-

- organization in natural swarms of photinus carolinus synchronous fireflies. *Science Advances*, 7(28):eabg9259, 2021.
- [48] John Buck. Synchronous rhythmic flashing of fireflies. ii. *The Quarterly review of biology*, 63(3):265–289, 1988.
- [49] Yaron Penn, Menahem Segal, and Elisha Moses. Network synchronization in hippocampal neurons. *Proceedings of the National Academy of Sciences*, 113(12):3341–3346, 2016.
- [50] Eli Ben-Naim. Opinion dynamics: rise and fall of political parties. *EPL (Europhysics Letters)*, 69(5):671, 2005.
- [51] Tamas Vicsek. A question of scale. *Nature*, 411(6836):421–421, 2001.
- [52] Carlos Delgado-Mata, Jesus Ibanez Martinez, Simon Bee, Rocio Ruiz-Rodarte, and Ruth Aylett. On the use of virtual animals with artificial fear in virtual environments. *New Generation Computing*, 25(2):145–169, 2007.
- [53] Rafael G Braga, Roberto C Da Silva, Alexandre CB Ramos, and Felix Mora-Camino. Collision avoidance based on reynolds rules: A case study using quadrotors. In *Information Technology-New Generations: 14th International Conference on Information Technology*, pages 773–780. Springer, 2018.
- [54] James Kennedy and Russell Eberhart. Particle swarm optimization. In *Proceedings of ICNN’95-international conference on neural networks*, volume 4, pages 1942–1948. IEEE, 1995.
- [55] Christopher Hartman and Bedrich Benes. Autonomous boids. *Computer Animation and Virtual Worlds*, 17(3-4):199–206, 2006.
- [56] Ruiwen Shu and Eitan Tadmor. Anticipation breeds alignment. *Archive for Rational Mechanics and Analysis*, 240:203–241, 2021.
- [57] José A Carrillo, Maria R D’Orsogna, and Vladislav Panferov. Double milling in self-propelled swarms from kinetic theory. *Kinetic and Related Models*, 2:363–378, 2009.
- [58] Gil Ariel and Amir Ayali. Locust collective motion and its modeling. *PLOS Computational Biology*, 11(12):e1004522, 2015.
- [59] Jerome Buhl, David JT Sumpter, Iain D Couzin, Joe J Hale, Emma Despland, Edgar R Miller, and Steve J Simpson. From disorder to order in marching locusts. *Science*, 312(5778):1402–1406, 2006.
- [60] Steven G Wilson. Basking sharks (cetorhinus maximus) schooling in the southern gulf of maine. *Fisheries Oceanography*, 13(4):283–286, 2004.
- [61] Malet-Engra Gema, Yu Weimiao, Oldani Admanda, Rey-Barroso Javier, Gov Nir S., Scita Giorgio, and Dupré Loïc. Collective cell motility promotes chemotactic prowess and resistance to chemorepulsion. *Curr Biol.*, 25(2):242 – 250, 2015.
- [62] Katherine Copenhagen, Gema Malet-Engra, Weimiao Yu, Giorgio Scita, Nir Gov, and Ajay Gopinathan. Frustration-induced phases in migrating cell clusters. *Science Advances*, 4(9):eaar8483, 2018.
- [63] Theodore Christian Schneirla et al. A unique case of circular milling in ants, considered in relation to trail following and the general problem of orientation. *American Museum Novitates*, 1253, 1944.
- [64] Pavlos Antoniou, Andreas Pitsillides, Tim Blackwell, Andries Engelbrecht, and Loizos Michael. Congestion control in wireless sensor networks based on bird flocking behavior. *Computer Networks*, 57(5):1167–1191, 2013.
- [65] M Hajihassani, D Jahed Armaghani, and R Kalatehjari. Applications of particle swarm optimization in geotechnical engineering: a comprehensive review. *Geotechnical and Geological Engineering*, 36(2):705–722, 2018.
- [66] Gábor Vásárhelyi, Csaba Virágh, Gergő Somorjai, Tamás Nepusz, Agoston E Eiben, and Tamás Vicsek. Optimized flocking of autonomous drones in confined environments. *Science Robotics*, 3(20):eaat3536, 2018.
- [67] Yongcan Cao, Wenwu Yu, Wei Ren, and Guanrong Chen. An overview of recent progress in the study of distributed multi-agent coordination. *IEEE Transactions on Industrial informatics*, 9(1):427–438, 2012.
- [68] Reza Olfati-Saber. Flocking for multi-agent dynamic systems: Algorithms and theory. *IEEE Transactions on automatic control*, 51(3):401–420, 2006.
- [69] Iain D Couzin. Collective cognition in animal groups. *Trends in cognitive sciences*, 13(1):36–43, 2009.
- [70] Søren Vedel, Savaş Tay, Darius M Johnston, Henrik Bruus, and Stephen R Quake. Migration of cells in a social context. *Proceedings of the National Academy of Sciences*, 110(1):129–134, 2013.
- [71] Lei Qin, Dazhi Yang, Weihong Yi, Huiling Cao, and Guozhi Xiao. Roles of leader and follower cells in collective cell migration. *Molecular biology of*

- the cell, 32(14):1267–1272, 2021.
- [72] Michael Vaughan Brian. Social insects: ecology and behavioural biology. Springer Science & Business Media, 2012.
- [73] Tim Clutton-Brock. Mammal societies. John Wiley & Sons, 2016.
- [74] Gladys Alexandre. Chemotaxis control of transient cell aggregation. Journal of bacteriology, 197(20):3230–3237, 2015.
- [75] Rosanna Man Wah Chau, Devaki Bhaya, and Kerwyn Casey Huang. Emergent phototactic responses of cyanobacteria under complex light regimes. MBio, 8(2):e02330–16, 2017.
- [76] Tristan Ursell, Rosanna Man Wah Chau, Susanne Wisen, Devaki Bhaya, and Kerwyn Casey Huang. Motility enhancement through surface modification is sufficient for cyanobacterial community organization during phototaxis. PLoS computational biology, 9(9):e1003205, 2013.
- [77] Mathieu Poujade, Erwan Grasland-Mongrain, A Hertzog, J Jouanneau, Philippe Chavier, Benoît Ladoux, Axel Buguin, and Pascal Silberzan. Collective migration of an epithelial monolayer in response to a model wound. Proceedings of the National Academy of Sciences, 104(41):15988–15993, 2007.
- [78] Nir S Gov. Collective cell migration patterns: follow the leader. Proceedings of the National Academy of Sciences, 104(41):15970–15971, 2007.
- [79] Ladoux Benoit and Mége René-Marc. Mechanobiology of collective cell behaviours. Nature reviews Molecular cell biology, 18(12):743–757, 2017.
- [80] Shuvasree SenGupta, Carole A Parent, and James E Bear. The principles of directed cell migration. Nature Reviews Molecular Cell Biology, 22(8):529–547, 2021.
- [81] Tomer J Czaczkes, Christoph Grüter, and Francis LW Ratnieks. Trail pheromones: an integrative view of their role in social insect colony organization. Annual review of entomology, 60:581–599, 2015.
- [82] Andrea Perna, Boris Granovskiy, Simon Garnier, Stamatios C Nicolis, Marjorie Labédan, Guy Theraulaz, Vincent Fourcassié, and David JT Sumpter. Individual rules for trail pattern formation in argentine ants (*linepithema humile*). PLoS computational biology, 8(7):e1002592, 2012.
- [83] Deborah M Gordon et al. The ecology of collective behavior in ants. Annu. Rev. Entomol., 64:35–50, 2019.
- [84] Ofer Feinerman, Itai Pinkoviezky, Aviram Gelblum, Ehud Fonio, and Nir S Gov. The physics of cooperative transport in groups of ants. Nature Physics, 14(7):683–693, 2018.
- [85] Eric Theveneau and Claudia Linker. Leaders in collective migration: are front cells really endowed with a particular set of skills? F1000Research, 6, 2017.
- [86] Kasia Kozyska, Giulia Pilia, Medhavi Vishwakarma, Laura Wagstaff, Maja Goschorska, Silvia Cirillo, Saad Mohamad, Kelli Gallacher, Rafael E Carazo Salas, and Eugenia Piddini. p53 directs leader cell behavior, migration, and clearance during epithelial repair. Science, 375(6581):eabl8876, 2022.
- [87] Francesco Bullo. Lectures on network systems, volume 1. Kindle Direct Publishing Santa Barbara, CA, 2019.
- [88] Herbert Levine, Wouter-Jan Rappel, and Inon Cohen. Self-organization in systems of self-propelled particles. Physical Review E, 63(1):017101, 2000.
- [89] Maria R D’Orsogna, Yao-Li Chuang, Andrea L Bertozzi, and Lincoln S Chayes. Self-propelled particles with soft-core interactions: patterns, stability, and collapse. Physical review letters, 96(10):104302, 2006.
- [90] Hugues Chaté, Francesco Ginelli, Guillaume Grégoire, and Franck Raynaud. Collective motion of self-propelled particles interacting without cohesion. Physical Review E, 77(4):046113, 2008.
- [91] Yao-Li Chuang, Maria R D’orsogna, Daniel Marthaler, Andrea L Bertozzi, and Lincoln S Chayes. State transitions and the continuum limit for a 2d interacting, self-propelled particle system. Physica D: Nonlinear Phenomena, 232(1):33–47, 2007.
- [92] Piotr Minakowski, Piotr B Mucha, Jan Peszek, and Ewelina Zatorska. Singular cucker–smale dynamics. In Active Particles, Volume 2, pages 201–243. Springer, 2019.
- [93] Young-Pil Choi, Dante Kalise, Jan Peszek, and Andrés A Peters. A collisionless singular cucker–smale model with decentralized formation control. SIAM Journal on Applied Dynamical Systems, 18(4):1954–1981, 2019.
- [94] José A Carrillo, Massimo Fornasier, Jesús Rosado, and Giuseppe Toscani. Asymptotic flocking dynamics for the kinetic cucker–smale model. SIAM Journal on Mathematical Analysis, 42(1):218–236, 2010.
- [95] José A Carrillo, Massimo Fornasier, Giuseppe

- Toscani, and Francesco Vecil. Particle, kinetic, and hydrodynamic models of swarming. Mathematical modeling of collective behavior in socio-economic and life sciences, pages 297–336, 2010.
- [96] José Antonio Carrillo, Young-Pil Choi, and Maxime Hauray. The derivation of swarming models: mean-field limit and wasserstein distances. Collective dynamics from bacteria to crowds, 553:1–46, 2014.
- [97] Young-Pil Choi, Seung-Yeal Ha, and Zhuchun Li. Emergent dynamics of the cucker–smale flocking model and its variants. Active Particles, Volume 1: Advances in Theory, Models, and Applications, pages 299–331, 2017.
- [98] Jaemann Park, H Jin Kim, and Seung-Yeal Ha. Cucker-smale flocking with inter-particle bonding forces. IEEE Transactions on Automatic Control, 55(11):2617–2623, 2010.
- [99] Guy A Djokam and Muruhan Rathinam. A generalized model of flocking with steering. SIAM Journal on Applied Dynamical Systems, 21(2):1352–1381, 2022.
- [100] K. Ha S.Y., Lee and Levy D. A simple proof of the cucker-smale flocking dynamics and mean-field limit. Commun. Math. Sci., 7(2):453–469, 2009.
- [101] Amanda Galante, Susanne Wisen, Devaki Bhaya, and Doron Levy. Stochastic models and simulations of phototaxis. Unifying Themes in Complex Systems, 8:105–119, 2011.
- [102] Seung-Yeal Ha and Doron Levy. Particle, kinetic and fluid models for phototaxis. Discrete Contin. Dyn. Syst. Ser. B, 12(1):77–108, 2009.
- [103] Devaki Bhaya, Doron Levy, and Tiago Requeijo. Group dynamics of phototaxis: Interacting stochastic many-particle systems and their continuum limit. In Hyperbolic Problems: Theory, Numerics, Applications, pages 145–159. Springer, 2008.
- [104] Doron Levy and Tiago Requeijo. Modeling group dynamics of phototaxis: from particle systems to pdes. Discrete and Continuous Dynamical Systems Series B, 9(1):103, 2008.
- [105] Doron Levy and Tiago Requeijo. Stochastic models for phototaxis. Bulletin of Mathematical Biology, 70:1684–1706, 2008.
- [106] Douglas D Risser and John C Meeks. Comparative transcriptomics with a motility-deficient mutant leads to identification of a novel polysaccharide secretion system in *n. ostoc punctiforme*. Molecular microbiology, 87(4):884–893, 2013.
- [107] Shakti N Menon, P Varuni, and Gautam I Menon. Information integration and collective motility in phototactic cyanobacteria. PLoS Computational Biology, 16(4):e1007807, 2020.
- [108] M Ben Amar. Collective chemotaxis and segregation of active bacterial colonies. Scientific Reports, 6(1):21269, 2016.
- [109] Evelyn F Keller and Lee A Segel. Model for chemotaxis. Journal of theoretical biology, 30(2):225–234, 1971.
- [110] Evelyn F Keller and Lee A Segel. Traveling bands of chemotactic bacteria: a theoretical analysis. Journal of theoretical biology, 30(2):235–248, 1971.
- [111] Ricard Alert, Alejandro Martínez-Calvo, and Sujit S Datta. Cellular sensing governs the stability of chemotactic fronts. Physical review letters, 128(14):148101, 2022.
- [112] Jackie Shen. Cucker–smale flocking under hierarchical leadership. SIAM Journal on Applied Mathematics, 68(3):694–719, 2008.
- [113] Jinliang Shao, Wei Xing Zheng, Ting-Zhu Huang, and Adrian N Bishop. On leader–follower consensus with switching topologies: An analysis inspired by pigeon hierarchies. IEEE Transactions on Automatic Control, 63(10):3588–3593, 2018.
- [114] Matteo Aureli and Maurizio Porfiri. Coordination of self-propelled particles through external leadership. Europhysics Letters, 92(4):40004, 2010.
- [115] Mark Shirley, Shlomovitz Roie, Gov Nir S., Roujade Mathieu, Grasland-Mongrain Erwan, and Silberzan Pascal. Physical model of the dynamic instability in an expanding cell culture. Biophys J., 98(3):361 – 370, 2010.
- [116] Tarle Victoria, Ravasio Andrea, Hakim Vincent, and Gov Nir S. Modeling the finger instability in an expanding cell monolayer. Integr Biol (Camb), 7(10):1218 – 1227, 2015.
- [117] Victoria Tarle, Estelle Gauquelin, Sri Ram Krishna Vedula, Joseph d’Alessandro, Chwee Teck Lim, Benoît Ladoux, and Nir S. Gov. Modeling collective cell migration in geometric confinement. Physical Biology, 14, 2017.
- [118] Nils Schuerger, Tchern Lenn, Ronald Kampmann, Markus V Meissner, Tiago Esteves, Maja Temerinac-Ott, Jan G Korvink, Alan R Lowe, Conrad W Mullineaux, and Annegret Wilde. Cyanobacteria use micro-optics to sense light direction. Elife, 5:e12620, 2016.
- [119] Nikita Chernetsov, Alexander Pakhomov, Dmitry Kobylkov, Dmitry Kishkinev, Richard A Hol-

land, and Henrik Mouritsen. Migratory eurasian reed warblers can use magnetic declination to solve the longitude problem. Current Biology, 27(17):2647–2651, 2017.